Published online 4 January 2010

Nucleic Acids Research, 2010, Vol. 38, No. 7 ***2485–2497***
doi:10.1093/nar/gkp1191

Insight into the induction mechanism of the GntR/HutC bacterial transcription regulator YvoA

Marcus Resch[1], Emile Schiltz[2], Fritz Titgemeyer[3] and Yves A. Muller[1,*]

[1]Lehrstuhl für Biotechnik, Department of Biology, Friedrich-Alexander University Erlangen-Nuremberg, Henkestr. 91, D-91052 Erlangen, [2]Institut für Organische Chemie und Biochemie, University of Freiburg, Albertstr. 21, D-79104 Freiburg and [3]Lehrstuhl für Mikrobiologie, Department of Biology, Friedrich-Alexander University Erlangen-Nuremberg, Staudtstr. 5, D-91052 Erlangen, Germany

Received October 9, 2009; Revised December 2, 2009; Accepted December 7, 2009

Downloaded from https://academic.oup.com/nar/article-abstract/38/7/2485/3100518 by guest on 20 November 2018

ABSTRACT

YvoA is a GntR/HutC transcription regulator from *Bacillus subtilis* implicated in the regulation of genes from the *N*-acetylglucosamine-degrading pathway. Its 2.4-Å crystal structure reveals a homodimeric assembly with each monomer displaying a two-domain fold. The C-terminal domain, which binds the effector *N*-acetylglucosamine-6-phosphate, adopts a chorismate lyase fold, whereas the N-terminal domain contains a winged helix–turn–helix DNA-binding domain. Isothermal titration calorimetry and site-directed mutagenesis revealed that the effector-binding site in YvoA coincides with the active site of related chorismate lyase from *Escherichia coli*. The characterization of the DNA- and effector-binding properties of two disulfide-bridged mutants that lock YvoA in two distinct conformational states provides for the first time detailed insight into the allosteric mechanism through which effector binding modulates DNA binding and, thereby regulates transcription in a representative GntR/HutC family member. Central to this allosteric coupling mechanism is a loop-to-helix transition with the dipole of the newly formed helix pointing toward the phosphate of the effector. This transition goes in hand with the emergence of internal symmetry in the effector-binding domain and, in addition, leads to a 122° rotation of the DNA-binding domains that is best described as a jumping-jack-like motion.

INTRODUCTION

Bacteria are able to utilize a variety of different carbohydrates. The corresponding metabolic genes are tightly regulated by globally and specifically acting transcription factors (1,2). Catabolic enzymes are in general only synthesized when their substrate is present, and when otherwise preferred carbon sources are absent. The underlying regulatory mechanisms are referred to as induction, carbon catabolite repression and inducer exclusion (2).

N-acetylglucosamine (GlcNAc) is a ubiquitous monosaccharide derivative of glucose and an essential molecule for all forms of life. GlcNAc is in addition a preferred carbon source for many microorganisms as it provides both carbon and nitrogen (3). YvoA is a bacterial repressor from *Bacillus subtilis* implicated in the control of the genes encoding GlcNAc degradative and biosynthetic enzymes (2,4). This implication is based on *in silico* analyses revealing that YvoA shares a sequence identity of 38% with the well-studied DasR regulator of the antibiotic-producing soil bacterium *Streptomyces coelicolor* (3,5). DasR represents a master switch in a signaling cascade from the nutrient GlcNAc to antibiotic production. It does this by controlling genes of GlcNAc and chitin metabolism as well as of transcription factors for antibiotic synthesis (5).

YvoA and DasR probably recognize identical operator sequences, the so-called *dre* (*DasR responsive element*) sites (6). Conserved *dre* sites are found in the genome of *B. subtilis* within the promoter regions of the *nagA-nagB-yvoA* and of the *nagP* gene locus [(7); Titgemeyer and Rigali, unpublished data]. *nagP* encodes for a putative permease for GlcNAc while *nagA* and *nagB* encode the metabolic enzymes *N*-acetylglucosamine-6-phosphate deacetylase (NagA) and glucosamine-6-phosphate deaminase (NagB), thus favoring the production of fructose-6-phosphate that can then be further metabolized through glycolysis (8,9). It has been shown that transcription of *nagA* and *nagB* is induced by GlcNAc (10). Hence, the genomic position and the above-described analogy to DasR suggest that YvoA controls *nag* gene expression in *B. subtilis* (7).

*To whom correspondence should be addressed. Tel: +49 0 9131 85 23082; Fax: +49 0 9131 85 23080; Email: ymuller@biologie.uni-erlangen.de
Present address:
Fritz Titgemeyer, Fachbereich Oecotrophologie, Fachhochschule Muenster, Corrensstr. 25, D-48149 Muenster, Germany.

© The Author(s) 2010. Published by Oxford University Press.
This is an Open Access article distributed under the terms of the Creative Commons Attribution Non-Commercial License (http://creativecommons.org/licenses/by-nc/2.5), which permits unrestricted non-commercial use, distribution, and reproduction in any medium, provided the original work is properly cited.

YvoA and DasR belong to the GntR/HutC family of bacterial transcriptional regulators. Members of this family control various biological processes, including antibiotic production, sensing of nutritional status, growth, proliferation and development (3,6). The GntR/HutC proteins can be considered as molecular chimeras of two domains. At their N-terminus they contain a winged helix–turn–helix domain (wHTH) responsible for DNA binding as a common feature of all members of the large and disperse GntR superfamily of repressors (6,11,12). The C-terminal part contains a chorismate lyase-type UTRA domain, which in combination with the wHTH domain is characteristic for the HutC subfamily of regulators (13). Whereas chorismate lyase contains an active site (14), HutC transcription regulators lack any enzymatic activity in the C-terminal domain. They contain a ligand-binding pocket instead that allows HutC transcription regulators to specifically recognize a variety of different effector molecules. This domain encompasses an allosteric mechanism that alters the affinity of the remote DNA-binding domains for DNA upon effector binding. Allosteric regulation is a hallmark of all bacterial repressor proteins and enables them to function as molecular switches that turn gene transcription on or off (15).

Several crystal structures of individual HutC effector-binding domains have been determined so far (16,17, K.Tan, C.Hatzos, J.Abdullah and A.Joachimiak, Midwest Center for Structural Genomics (MCSG), unpublished data), and, recently, a single structure of an entire HutC repressor has become available as part of the MCSG structural genomics initiative. However, whereas for numerous repressor families, the allosteric mechanism by which effector binding modulates DNA binding is understood in atomic detail, as for instance the lactose (18,19) and tetracycline repressor system (15,20), in case of the HutC family, none of the structures solved so far allowed for the identification of either the effector-binding site or the allosteric mechanism by which these repressors exert their function.

Here, we describe for the first time the crystal structure of full-length YvoA in what we consider to constitute the induced conformation. The effector-binding site has been identified by site-directed mutagenesis, and the characterization of disulfide-bridge-containing mutants that lock YvoA in either the DNA-bound or the effector-bound induced conformation allows us to propose a 'jumping jack' model for the allosteric induction of YvoA.

MATERIALS AND METHODS

Protein cloning, mutagenesis, expression and purification

YvoA (BSU35030, UniProtKB/TrEMBL entry O34817) from *B. subtilis* and mutants thereof were expressed and purified as described (21). Amino acid exchanges were introduced by site-directed mutagenesis using the QuikChange site-directed mutagenesis kit (Stratagene, La Jolla, CA 92037, USA). The following YvoA single point mutants were generated: YvoA-I209E (using primers I209Eforw: GAGCGCCTGTCCTATTAGAAA AACGAACAACATATC, I209Erev: GATATGTT GTTCGTTTTTCTAATAGGACAGGCGCTC), I209L (I209Lforw: CGCCTGTCCTATTACTTAAACGAACA ACATATC, I209Lrev: GATATGTTGTTCGTTTAAGT AATAGGACAGGCG), E222D (E222Dforw: GAACGG AACTGCTTTTAACCATGCAAAATCCG, E222Drev: CGGATTTTGCATGGTTAAAAGCAGTTCCGTTC), A224R (A224Rforw: CGGAACTGCTTTTGAGCATCG TAAATCCGTATACAGAGGC, A224Rrev: GCCTCTG TATACGGATTTACGATGCTCAAAAGCAGT TCCG).

In addition, the following double-mutants were generated: YvoA-K24C-G97C (using primers K24Cforw: GCAATTAAAAACCCAAATTTGCAACGGAGAGCT GCAGCCGG, K24Crev: CCGGCTGCAGCTCTCCGT TGCAAATTTGGGTTTTTAATTGC; G97Cforw: GG ATATGAAAAGCCGCTGCATGACACCGGGCAGC AG, G97Crev: CTGCTGCCCGGTGTCATGCAG CGGCTTTTCATATCC), and YvoA-E61C-L242C (E61Cforw: GCGCTTTCTAATTTAGTTAATTGCGG CTTGCTCTATCGCCTGAAAG, E61Crev: CTTTCAG GCGATAGAGCAAGCCGCAATTAACTAAATTAG AAAGCGC; L242Cforw: CATTTGTCCACTATAT GGATCGTTGCTCATAAAAAAAGCCTCCAACCC, L242Crev: GGGTTGGAGGCTTTTTTTATGAGCAAC GATCCATATAGTGGACAAATG), performing two consecutive rounds of site-directed mutagenesis for each double mutant. After two-stage polymerase chain reaction (PCR) (22), the parent plasmid strands were digested with Dpn1 and the mutated strands chemically transformed into competent *Escherichia coli* XL10 Gold cells (Stratagene). Successful mutagenesis was confirmed by DNA sequence analysis.

For the production of selenomethionine substituted YvoA (SeMet-YvoA), cells were grown at 37°C to an OD_{600} of 0.5 in minimal medium M9 supplemented with 0.8% (*v*/*v*) glycerol, 100 μg ml^{-1} ampicillin, 10 μg ml^{-1} kanamycin and a feedback inhibition mix containing selenomethionine (23). After additional 15 min of shaking, the temperature was lowered to 20°C and protein expression induced with 1 mM IPTG. The purification protocol for SeMet-YvoA was the same as for the wild-type and mutant proteins except that the affinity chromatography buffers additionally contained 5 mM dithiothreitol. Protein concentrations were determined spectrophotometrically at 280 nm with a calculated molar extinction coefficient of 16 390 M^{-1} cm^{-1} and a molecular weight of 27.8 kDa. Typically, one litre of bacterial culture yielded about 50 mg of wild-type and SeMet-YvoA protein and about 10–40 mg of mutant protein.

Limited proteolysis assay

YvoA protein was incubated at 25°C at a concentration of 0.35 mg ml^{-1} (corresponding to 6 μM YvoA dimer) for time periods up to 3 h with the nonspecific serine protease subtilisin. The reaction buffer contained 20 mM Tris–HCl, pH 7.5, 0.15 M NaCl and a final amount of 0.014 U subtilisin per milligram YvoA. Digestion was performed in the presence or absence of 6 μM dsDNA

Downloaded from https://academic.oup.com/nar/article-abstract/38/7/2485/3100518 by guest on 20 November 2018

(duplexed ATTGGTATAGATCACTAG). Likewise, digestion was performed in the presence or absence of 1.5 mM GlcNAc-6-P. After 0.5, 1, 5, 15, 30, 60 and 180 min samples were withdrawn, and digestion was stopped by adding equal volumes of sodium dodecyl sulfate (SDS) sample buffer. Samples were immediately boiled and examined by SDS gel electrophoresis.

Isothermal titration calorimetry

Calorimetric titrations of YvoA with GlcNAc-6-P were performed with a VP-isothermal titration calorimetry (ITC) microcalorimeter (MicroCal, Northampton, MA 01060, USA). Protein samples were extensively dialyzed against ITC buffer containing 20 mM sodium phosphate (pH 7.5) and 150 mM NaCl. All solutions were filtered using membrane filters (pore size 0.22 μm) and degassed for 30 min by gently stirring under vacuum. The 1.35-ml sample cell was filled with a 30 μM solution of protein (calculated for monomeric protein) and the 250 μl injection syringe with a 10 or 20 mM solution of the effector. Each titration typically consisted of an initial 2-μl injection followed by 25 consecutive 10-μl injections at 25°C. Calorimetric titration of dsDNA with wild-type YvoA was performed similarly. The 1.35-ml sample cell was filled with a 12-μM solution of duplex DNA (ATTGGT ATAGATCACTAG) (7) and the 250-μl injection syringe with 125-μM wild-type YvoA (calculated for dimeric protein). Data for the initial injection, which are affected by diffusion of the solution from and into the injection syringe during the initial equilibration period, were discarded. Binding isotherms were generated by plotting the normalized reaction heats against the ratio of total injectant to total protein per injection. Integrated heat effects, after correction for heats of dilution, were analyzed by nonlinear regression with a one-site-binding model using the standard Microcal Origin 7.0 software package. Changes in free energy and entropy upon binding were calculated from the equilibrium parameters using the equation: $\Delta G^\circ = -RT\cdot\ln K = \Delta H^\circ - T\cdot\Delta S^\circ$, where R is the universal gas constant, T the temperature, K the association constant, ΔG° the change in Gibbs free energy, ΔH° the change in enthalpy and ΔS° is the change in entropy (24) under standard conditions.

Protein crystallization, data collection, structure determination and refinement

Selenomethionine-substituted YvoA was crystallized in the absence of the effector GlcNAc-6-P as described for native YvoA (21). Two diffraction data sets [Se-multiple wavelength anomalous dispersion (MAD)] were collected from a single SeMet-YvoA crystal at 100 K at synchrotron beam line BL14.2 of Free University Berlin at BESSY (Berlin, Germany) to maximum resolution of 2.4 Å. Peak data were collected at a wavelength of 0.97965 Å in 0.5° oscillation steps covering a total rotation range of 125°. Inflection data were collected at a wavelength of 0.97979 Å, accordingly. Data were indexed and integrated with XDS and scaled with XSCALE (25). The structure was solved by the MAD method using program AUTOSHARP (26). A polyalanine model generated from the homolog PhnF C-terminal domain (PDB code: 2FA1) (16) was placed manually into the electron density using the program COOT (27). The orientation of the C-terminal domains was fitted by rigid body refinement using REFMAC5 (28). The model was completed and corrected manually using COOT and by alternating with automated cycles of restrained atom position and individual *B*-factor refinement with REFMAC5 (28). Noncrystallographic symmetry restraints were defined for two groups of residues (residues 1–77 and 78–242) and applied to all 10 copies in the asymmetric unit (chains A–J) during the refinement. Sulfate ions and water molecules were added in the final stages of the refinement. During the final stages of refinement, group atomic translation libration and skrew-rotation (TLS) displacement parameters were refined. The ten molecules in the asymmetric unit were divided into 70 TLS groups (Supplementary Table S1) as suggested by the TLS motion determination home page (30,31) (http://skuld.bmsc.washington.edu/~tlsmd/). The resulting TLS tensors were analyzed using TLSANL (32). A summary of the crystallographic data collection and refinement statistics is presented in Table 1. All structure depictions were generated using the program PYMOL (33). Coordinates for the YvoA crystal structure have been deposited in the Protein Data Bank (PDB, ID code 2WV0).

Homology modeling

YvoA in the DNA-bound conformation was modeled using the ESyPred3D (34) web server 1.0 (http://www.fundp.ac.be/sciences/biologie/urbm/bioinfo/esypred/). Chain A from the crystal structure of the putative transcriptional regulator YydK from *B. subtilis* (PDB code: 3BWG) (K.Tan, M.Zhou, J.Abdullah and A.Joachimiak, Midwest Center for Structural Genomics (MCSG), unpublished data) was identified as the best template for modeling. Superposition of the DNA-binding domains of the model obtained above onto the homologous DNA-binding domains from FadR bound to DNA (PDB code: 1HW2) (35) was calculated with the program LSQKAB (36).

RESULTS

Overall structure of YvoA

The crystal structure of YvoA was solved at 2.4 Å by MAD using selenomethionine substituted YvoA (Table 1). The crystals contain 10 molecules in the asymmetric unit. Intriguingly, these form five crystallographic dimers and are arranged along a 5_1 screw axis creating a left-handed helix with a pitch of ~160 Å and a ~25 Å diameter pore at its centre (Supplementary Figure S1 A and B). Of the 10 molecules (A–J), molecules A–F and I are defined best by their electron density, whereas molecules G, H and J lack density for some segments and display particularly high *B*-values in several surface exposed regions.

The N-terminal part of the protein (residues 1–76) contains a canonical wHTH DNA-binding domain with

Downloaded from https://academic.oup.com/nar/article-abstract/38/7/2485/3100518 by guest on 20 November 2018

Table 1. Crystal parameters, X-ray data collection, phasing and refinement statistics

	Selenomethionine YvoA crystal		
	Se *peak*	Se *inflection*	Se *native*
Data collection			
Beam line	BESSY-MX, BL14.2		
Wavelength (Å)	0.97965	0.97979	0.97965
Resolution (Å)	45.00–2.40 (2.50–2.40)	45.00–2.50 (2.60–2.50)	45.00–2.40 (2.50–2.40)
Space group	*C*2		
Cell parameters	$a = 208.41$, $b = 137.08$, $c = 120.19$ Å, $\beta = 94.97°$		
No. of molecules in the ASU	10		
$I/\sigma(I)$	9.2 (1.9)	10.8 (1.7)	6.5 (2.3)
R_{int}[a] (%)	4.4 (34.9)	4.1 (41.0)	8.4 (40.6)
R_{meas}[b] (%)	6.2 (49.3)	5.8 (57.9)	10.6 (51.1)
R_{mrgd}-F[b] (%)	13.2 (61.4)	13.6 (75.6)	15.2 (53.1)
Unique reflections	249 821	218 213	130 361
Redundancy	1.4	1.4	2.6
Completeness (%)	96.4 (96.6)	95.2 (92.2)	99.3 (100.0)
Wilson *B*-value (Å^2)	63.4	67.3	55.4
Solvent content (%)	59.9		
Phasing statistics (45.0–2.4 Å)			
No. of sites	81 (found) out of 90 (possible)		
Phasing power (ano, acentric)	1.696		
R_{Cullis}[c] (ano, acentric)	0.662		
FOM (acentric/centric)	0.432/0.210		
Refinement statistics (100.0–2.4 Å)			
$R_{work}/R_{free}/R_{total}$[d] (%)			19.9/25.6/20.5
Number of non-hydrogen atoms			18 689
Number of residues			2378
Number of solvent molecules			769
Additional molecules			15 SO_4^{2-}
No. of TLS groups used in refinement			70
Overall mean *B*-value (Å^2)			64.5
Mean *B*-value of 10 protein chains (Å^2)			65.4
Mean *B*-value of sulfates (Å^2)			54.2
Mean *B*-value of water molecules (Å^2)			54.2
R.m.s.d. from ideal geometry			
Bond lengths (Å)			0.014
Bond angles (°)			1.251
Ramachandran statistics[e] (%)			92.5/7.4/0.1/0.0

[a] $R_{int} = \Sigma_{hkl} \Sigma_i |I_i(hkl) - \langle I(hkl)\rangle| / \Sigma_{hkl} \Sigma_i I_i(hkl)$, where $I_i(hkl)$ is the intensity measurement for reflection *hkl*, and $\langle I(hkl)\rangle$ is the mean intensity of crystallographically replicants and symmetry-related reflections.
[b] R_{meas} is the multiplicity weighted merging *R*-factor, and $R_{mrgd\text{-}F}$ is an indicator for the quality of the reduced data (47).
[c] $R_{Cullis} = \Sigma_{hkl} || \Delta_{ano,\ obs}| - |\langle\Delta_{ano,\ calc}\rangle|| / \Sigma_{hkl} || \Delta_{ano,\ obs}|$, where $\Delta_{ano,\ obs}$ and $\Delta_{ano,\ calc}$ are the observed and calculated anomalous differences (36).
[d] $R_{work}/R_{free}/R_{total} = 100\ (\Sigma_{hkl} |F_o(hkl) - F_c(hkl)| / \Sigma_{hkl} F_o(hkl))$, where F_o and F_c are the observed and calculated structure factor amplitudes, respectively. R_{free} is calculated for 10% of randomly selected reflections excluded from refinement.
[e] The Ramachandran statistics were obtained with the program PROCHECK (48). Reported is the percentage of residues in the most favored, additionally allowed, generally allowed and disallowed areas of the Ramachandran plot.

α1–β1–α2–α3–β2–β3 topology and is attached to the C-terminal domain via a 21 residue-long linker (residues 77–97; Figure 1A and B). The C-terminal effector-binding domain displays a chorismate lyase fold and contains a six-stranded antiparallel β-sheet in its core (β4–9), which is extended on one side by β-strand β10 from a second monomer. The C-terminal domain displays a remarkable topology as it contains a 2-fold internal repeat comprising one-half of the central β-sheet and one-half of all flanking helices. The repeats are related by a pseudo 2-fold symmetry axis that intersects with a bound sulfate ion (sulfate-binding site 1, Figure 1C). This sulfate is located on top of the central β-sheet flanked by the helices α5 and α9 and occurs in all YvoA monomers with the exception of monomers H and J that display overall poorer density. An additional sulfate-binding site (sulfate-binding site 2) could be identified at the N-terminal end of helix α1 (Figure 1B). Again, this site is not occupied in all of the 10 molecules, and in total, the model contains 15 sulfates. The N- to C-terminal inter-domain orientation is highly conserved in all copies of YvoA in the crystal (Supplementary Figure S1C). The average root-mean-square deviation (r.m.s.d.) for the pairwise superposition of the C_α atoms of all 10 monomers is 1.02 Å, suggesting that this orientation corresponds to a low-energy conformation in YvoA.

The YvoA molecules dimerize via their effector-binding domains (Figure 1A) burying an average interface area of 1700 Å^2 per monomer. Dimerization is achieved via hydrogen bonds formed between β-strands β7 and β10′ and via salt bridges (between residues R241-E91′, D240-R180′, E171-R241′). Dimer formation can also be monitored in solution, namely by gel filtration (21) and chemical cross-linking employing formaldehyde and

Downloaded from https://academic.oup.com/nar/article-abstract/38/7/2485/3100518 by guest on 20 November 2018

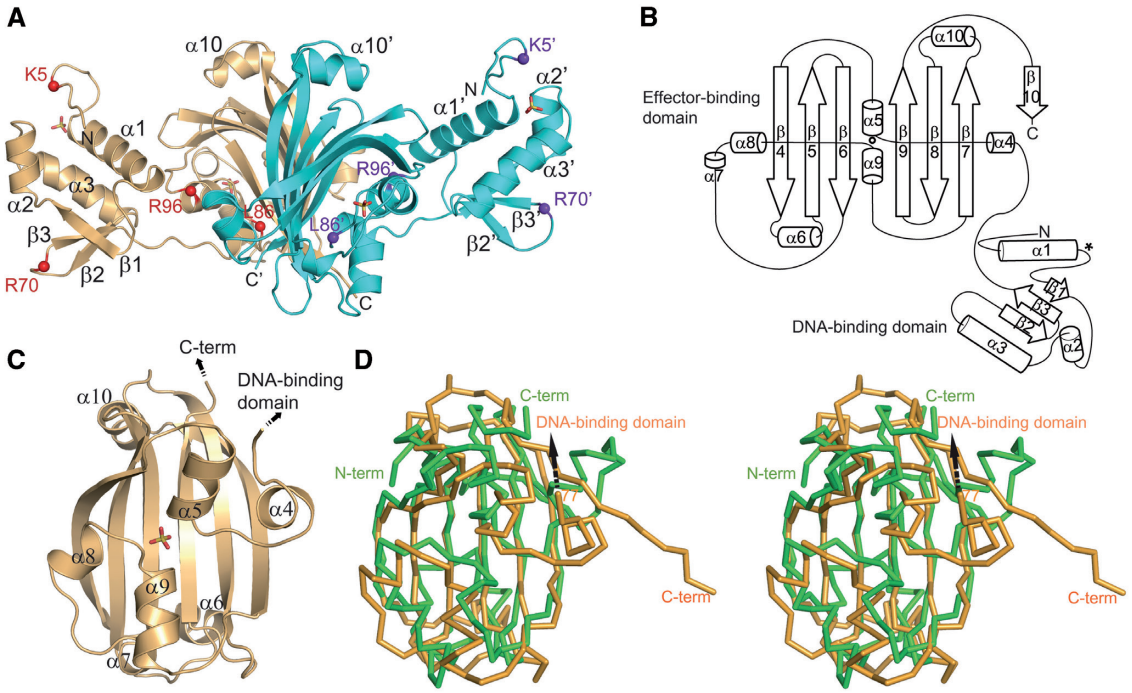

Figure 1. Key structural features of YvoA from *Bacillus subtilis*. (**A**) Crystal structure of the YvoA homodimer (orange/cyan) at 2.4-Å resolution with bound sulfate ions. Residues/positions susceptible to proteolytic cleavage are marked in red and purple. (**B**) Topology plot of the YvoA monomer. Circle and asterisk mark the sulfate-binding sites 1 and 2, respectively. (**C**) Ribbon representation of the effector-binding domain highlighting the internal 2-fold rotational symmetry of the fold. The 2-fold axis passes through the sulfate ion that is hold in place by helices α5 and α9. (**D**) Stereo view of the superimposition of the effector-binding domain of YvoA (orange) and chorismate lyase from *E. coli* (in green, PDB code: 1G1B) (14).

glutardialdehyde (data not shown). The YvoA dimerization mode is identical to that observed in crystal structures of individual effector-binding domains of GntR/HutC family members such as in PhnF (PDB code: 2FA1) (16), TreR (PDB code: 2OGG) (17) and YurK from *B. subtilis* (PDB code: 2IKK) (K.Tan, C.Hatzos, J.Abdullah and A.Joachimiak, Midwest Center for Structural Genomics (MCSG), unpublished data) as well as in full-length YydK (PDB code: 3BWG) (K.Tan, M.Zhou, J.Abdullah and A.Joachimiak, Midwest Center for Structural Genomics (MCSG), unpublished data), which suggests that the observed dimerization mode is characteristic for the GntR/HutC family of bacterial repressors.

The program *DaliLite* (http://ekhidna.biocenter.helsinki.fi/dali_server) (37) reported 27 different entries with *Z*-scores >10 as close structural neighbors of YvoA. The nearest neighbor was identified as the uncharacterized gene product SA0254 from *Staphylococcus aureus* (PDB code: 2OOI) [R. Zhang, E.Duggan, M.Gu, and A.Joachimiak, Midwest Center for Structural Genomics (MCSG), unpublished data] (r.m.s.d. = 1.8 Å, sequence identity = 22%) and the second closest neighbor as YydK from *B. subtilis* (PDB code: 3BWG) (PDB code: 2OOI) (r.m.s.d. = 2.0 Å, sequence identity = 27%). The *E. coli* enzyme chorismate lyase (PDB code: 1G1B) (14) was identified at position 21 (r.m.s.d. of 3.0 Å and a global sequence identity of 14%; for a superposition see Figure 1D). All entries corroborate the observation that the occurrence of the fold of the effector-binding domain is restricted to either enzymes or to the GntR/HutC family, of which YvoA appears to be a representative member (13,14,38).

The YvoA effector-binding site coincides with the active site of chorismate lyase

HutC family members are expected to bind a variety of different effector molecules but until now no structural insight is available on any such complexes. In chorismate lyase, eponymous for the fold of the effector-binding domain, the active site is located on top of the central β-sheet near the geometric centre of the enzyme (13,14). In YvoA, we observe a sulfate ion bound at an equivalent position (Figure 1C). The sulfate is bound via the N-termini of helices α5 and α9, by the guanidinium groups of R133 and R135, by the hydroxyl groups of T90 and S165, and by the backbone amides of F89, S165, I166 and Y167 (Figure 2).

We hypothesized that this sulfate ion occupies the position at which low-molecular-weight effectors interact with YvoA. As glucosamine-6-phosphate (GlcN-6-P) has been identified as the effector of the YvoA homolog DasR (3), and because both proteins are implicated in the regulation of the GlcNAc metabolism, we reasoned that GlcN-6-P might also be the effector of YvoA. Therefore, we probed wild-type YvoA for binding GlcN-6-P as well as the related molecule *N*-acetylglucosamine-6-phosphate (GlcNAc-6-P). Only for the latter, we were able to obtain interpretable ITC-binding curves yielding a dissociation constant of 1 mM (K_d) (Table 2, Figure 2A). This

Downloaded from https://academic.oup.com/nar/article-abstract/38/7/2485/3100518 by guest on 20 November 2018

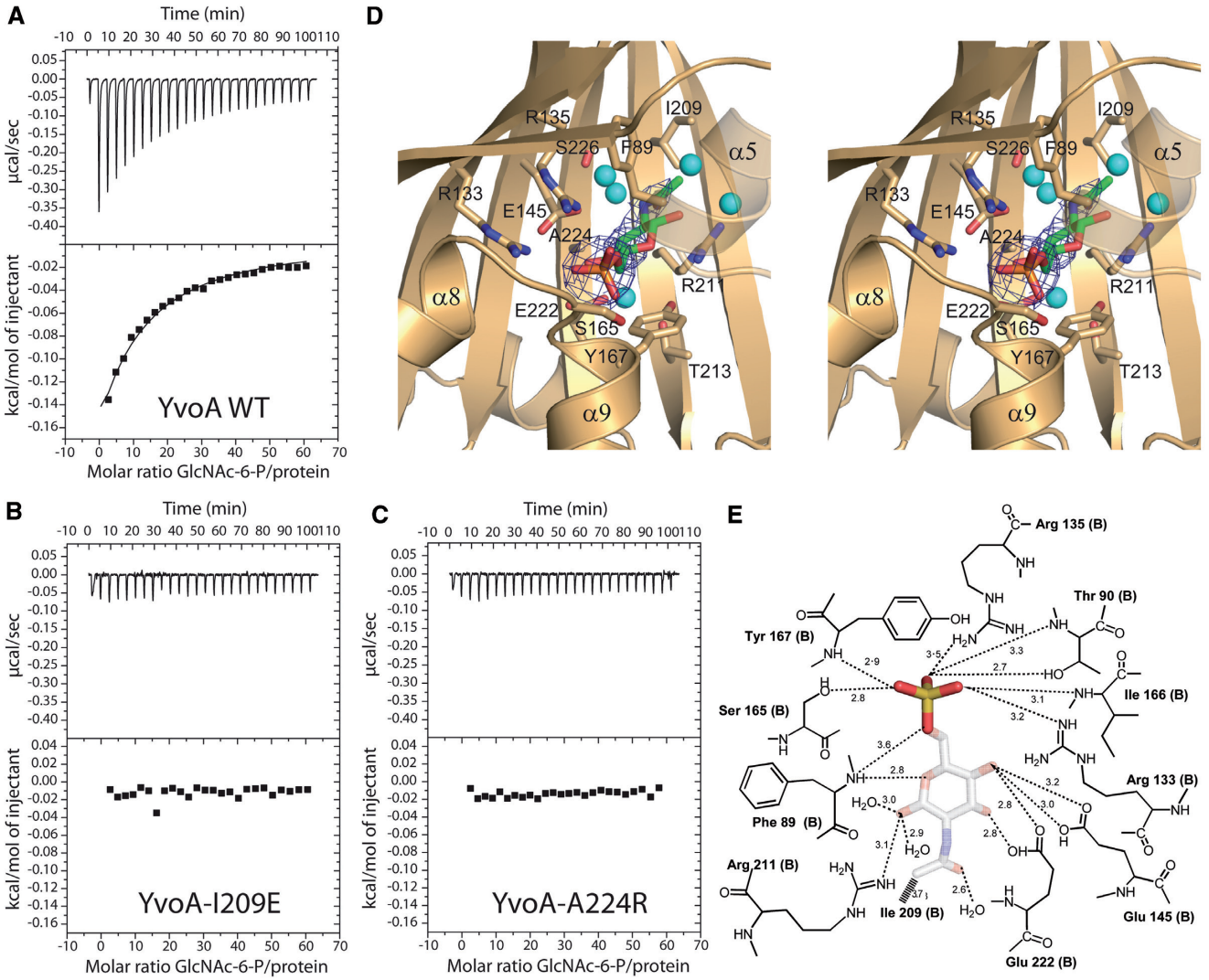

Figure 2. GlcNAc-6-P effector binding to YvoA. (**A–C**) Binding isotherms of YvoA and YvoA mutants (0.9 mg ml^{-1}) titrated with 10 mM GlcNAc-6-P. (A) Wild-type YvoA, (B) YvoA-I209E and (C) YvoA-A224R. (**D**) Stereo view showing the proposed effector-binding site of YvoA. GlcNAc-6-P in β-configuration can be docked into weak non-protein electron density present in the initial MAD-phased experimental electron density map near monomer B (in blue). (**E**) Schematic representations of the interactions between GlcNAc-6-P and side-chains from the effector-binding site of YvoA (chain B). GlcNAc-6-P is not part of the deposited refined crystal structure and is therefore colored transparently. The position of the sulfate coincides with that of the phosphate group of GlcNAc-6-P.

represents a relatively weak binding affinity and could indicate that yet unknown YvoA effectors with higher affinities exist. On the other hand, when considering that the intracellular concentrations of GlcNAc-6-P lie in the range of 1–10 mM under GlcNAc catabolizing conditions (Fritz Titgemeyer, personal communication), a high occupancy of the effector-binding site can be achieved despite the low overall affinity of GlcNAc-6-P.

To unambiguously identify the GlcNAc-6-P-binding site, we generated several point mutants and tested their ability to bind GlcNAc-6-P (Table 2). Proper folding of each mutant was confirmed by circular dichroism (CD) spectroscopy (Supplementary Figure S2 A and B). Introducing small changes in the side-chains near the bound sulfate ion caused no or little effects on GlcNAc-6-P binding (mutants E222D and I209L, Supplementary Figure S3 A and B). Introduction of bulky and charged side-chains abolished GlcNAc-6-P binding completely (mutants I209E and A224R, Figure 2B and C).

An additional clue that the sulfate and effector-binding sites coincide can be derived from residual electron density in the initial MAD-phased experimental density map near monomer B that cannot be ascribed to the protein (Figure 2D). Guided by this density, GlcNAc-6-P could be docked into the binding site without any steric clashes. In addition to the interactions of the phosphoryl group of GlcNAc-6-P, which are identical to those of the sulfate molecule, GlcNAc-6-P is able to establish numerous hydrogen bonds, mainly via side-chain atoms, together with a few hydrophobic contacts such as that found between Y167 and C_6 of the glucose moiety (Figure 2D and E). Close inspection of the proposed binding mode also reveals striking similarity to the binding mode of

Downloaded from https://academic.oup.com/nar/article-abstract/38/7/2485/3100518 by guest on 20 November 2018

Table 2. Effector and DNA-binding affinities determined by ITC

	K_d (M)	n	$\Delta H^{\circ a}$	$\Delta G^{\circ a}$	$T\Delta S^{\circ a}$
GlcNAc-6-P was titrated to					
Wild-type YvoA	$1.0 \cdot 10^{-3}$	1[b]	–18.9	–17.1	–1.8
YvoA-E222D	$1.1 \cdot 10^{-3}$	1[b]	–21.2	–17.0	–4.2
YvoA-I209L	$3.3 \cdot 10^{-3}$	1[b]	–35.9	–14.2	–21.7
YvoA-I209E	No binding observed	–	–	–	–
YvoA-A224R	No binding observed	–	–	–	–
YvoA-E61C-L242C	No binding observed	–	–	–	–
YvoA-K24C-G97C	$1.8 \cdot 10^{-3}$	1[b]	–16.8	–15.6	–1.2
Wild-type YvoA was titrated to					
dsDNA (18mer)	$131.2 \cdot 10^{-9}$	1[c]	26.9	–39.3	66.2
dsDNA was titrated to					
Wild-type YvoA	$2.9 \cdot 10^{-9}$ (K_{d1})	n_1 0.47[c]	ΔH°_1 –26.4	ΔG°_1 –48.7	$T\Delta S^{\circ}_1$ 22.3
	$0.5 \cdot 10^{-6}$ (K_{d2})	n_2 0.44[c]	ΔH°_2 70.0	ΔG°_2 –36.1	$T\Delta S^{\circ}_2$ 106.1

[a]Units are in kJ mol^{-1}.
[b]This stoichiometry factor refers to an YvoA monomer.
[c]This stoichiometry factor refers to dimeric YvoA.

GlcNAc-6-P in *N*-acetylglucosamine-phosphate mutase (PDB code: 2DKC; (39); Supplementary Figure S4), despite the fact that the folds of the two proteins are unrelated. Any trial calculations aiming at including GlcNAc-6-P into the crystallographic refinement remained unsuccessful and no unambiguous electron density was obtained for the glucose moiety of the ligand after refinement. Therefore, only the bound sulfate molecule was included in the final structure. Any attempts to obtain a GlcNAc-6-P-bound structure of YvoA failed so far.

Interestingly, the crystal structures of the related HutC members trehalose repressor TreR of *B. subtilis* (PDB code: 2OGG) (17) and YurK from *B. subtilis* (PDB code: 2IKK) contain also a sulfate ion at the same position. Even the corresponding residues R128 and R130 are conserved in TreR and YurK (R130 is replaced by a histidine in YurK). In TreR it has been proposed that the sulfate mimics the phosphoryl group of the effector trehalose-6-phosphate (17). From a structural point of view, it is not uncommon that an anion binds to the N-termini of two α-helices as it is well known that α-helices are able to favor the binding of negatively charged ligands at this position either via the helix dipole or/and via direct hydrogen-bond donation (40–42). It is quite likely that the high sulfate concentration used during crystallization (21) led to the occupancy of the GlcNAc-6-P-binding site by sulfate ions. Moreover, since effector binding leads to the induction of YvoA, the possibility must be considered that the observed structure of YvoA represents the induced conformation with impaired DNA operator-binding capability.

YvoA binds DNA in a two-step mechanism

YvoA has been proposed to recognize the natural occurring operator sequence ATTGGTATAGATCACT AG from *B. subtilis* (7), which is highly similar to the common *dre* sites found in *S coelicolor* (43). We investigated DNA binding of YvoA using this double-stranded DNA (dsDNA) and analytical gel filtration chromatography (Figure 3A). When dimeric wild-type YvoA is added in equimolar amounts to dsDNA, the YvoA–DNA complex elutes as a DNA-bound YvoA dimer. In contrast, when YvoA is added in 3.5-fold molar excess over dsDNA, a tetrameric state is observed (two YvoA dimers bind to one dsDNA, Figure 3A). The oligomeric states were determined by linear regression employing a calibration curve. In order to further characterize DNA binding, ITC was conducted with the same dsDNA by titrating YvoA to DNA (Supplementary Figure S5A, Table 2). The binding revealed an apparent K_d of 131.2 nM. Inversely, when dsDNA was titrated to YvoA, a biphasic isotherm was observed with two different K_d values revealing negative co-operativity (Supplementary Figure S5B, Table 2). This suggests a two-step-binding mechanism for YvoA. In the first step and in the presence of excessive YvoA, two YvoA dimers bind to one molecule of dsDNA via only one of the two DNA-binding domains present in each dimer. In the subsequent step, and upon increasing the DNA concentrations, one YvoA dimer dissociates from the complex and the remaining dimer now contacts the dsDNA with both binding domains. In case when dsDNA is present in excess, the complex of a YvoA dimer bound to dsDNA is formed from the onset.

It is not possible to explain the formation of a 1:1 complex between dimeric YvoA and dsDNA on the basis of the YvoA crystal structure since in the structure the DNA-binding domains are splayed apart so that they cannot contact both half-sites of a single operator site simultaneously. To obtain a structural model of YvoA that would allow for the formation of such a complex, we considered the structure of the homolog transcriptional regulator YydK from *B. subtilis* (PDB code: 3BWG). YydK exhibits 27% sequence identity to YvoA, and its DNA-binding domains are oriented differently than in YvoA. They are paired together at the dimer interface and in this conformation the DNA recognition helices α3 and α3′ appear at the correct distance to bind into neighboring major grooves of dsDNA. This possibility is supported by a comparison of YydK with the crystal structure showing how the DNA-binding domains

Downloaded from https://academic.oup.com/nar/article-abstract/38/7/2485/3100518 by guest on 20 November 2018

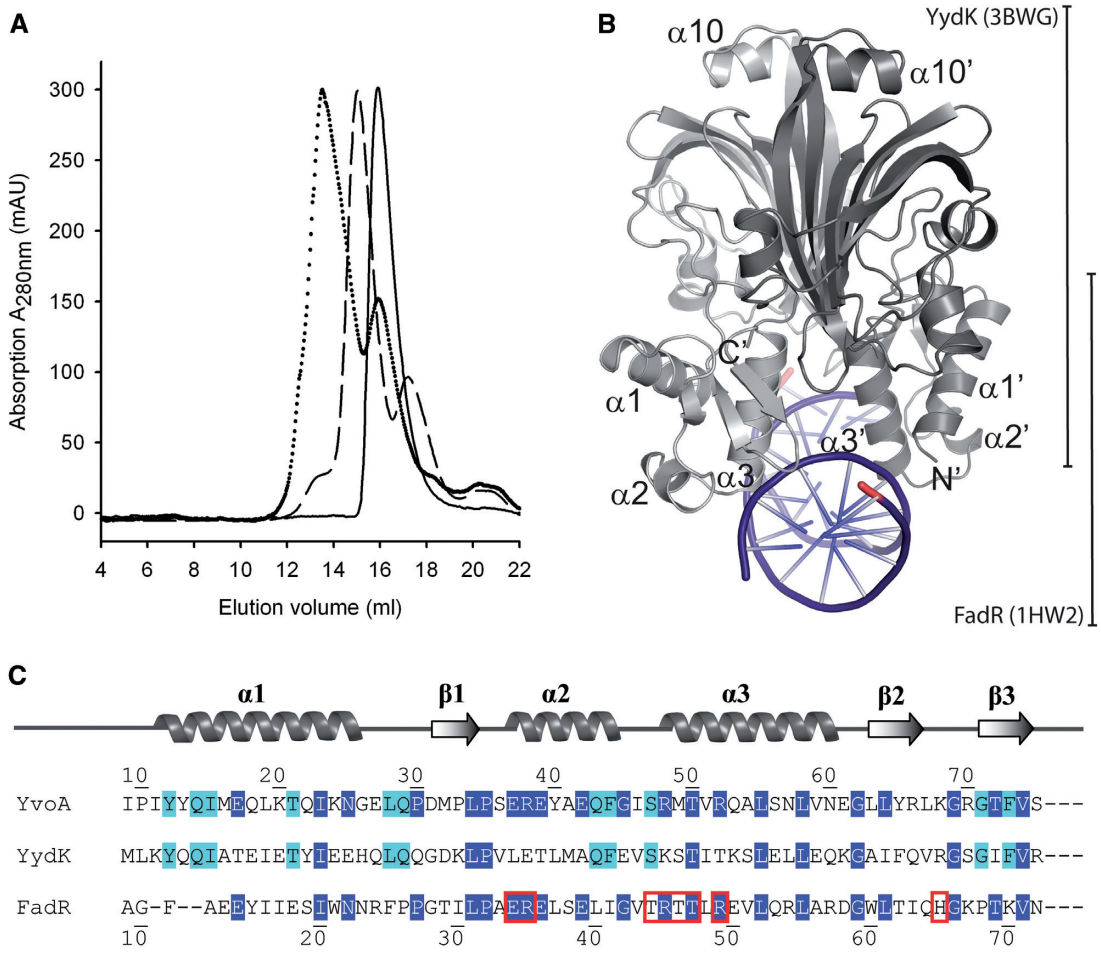

Figure 3. DNA-binding properties of YvoA. (**A**) Gel filtration of YvoA (solid line), upon addition of equimolar dsDNA (dashed line), and with YvoA in excess over dsDNA (dotted line) demonstrating clear shifts of the elution peaks as a function of the protein:DNA ratio. (**B**) Ribbon representation of a DNA-bound YvoA model. The composite model was generated by modeling YvoA according to the conformation observed in YydK (PDB code: 3BWG) and superimposed on the DNA-binding heads of the DNA-bound wHTH domains of FadR (PDB code: 1HW2) (35). (**C**) Sequence alignments of the DNA-binding domains of YvoA from *B. subtilis*, FadR from *E. coli*, and YydK from *B. subtilis*. The secondary structure elements, indicated by helices and arrows, refer to YvoA. Residues conserved between YvoA and FadR (and partially YydK) are highlighted by blue shaded boxes. Residues conserved only between YvoA and YydK are indicated by cyan shaded boxes. Residues implicated in DNA binding in FadR (35) are highlighted by red boxes.

of FadR from *E. coli* interact with dsDNA (35,44). The DNA-binding domain dimer of FadR can be superimposed with the corresponding domains of YydK with an r.m.s.d. of 5.3 Å for all C_α atoms. The deviations between single DNA-binding domains are significantly lower (1.6 Å). Although a C_α r.m.s.d. of 5.3 Å suggests notable differences in the dimer assembly, the overall orientation of the DNA-binding domains is very similar in both proteins. Any differences could originate either from the fact that YydK was crystallized in the absence of DNA or from the observation that the two operator half sites are separated by a different number of nucleotides in the operators of YydK/YvoA and FadR (Table 3). Consequently, a slightly different positioning of the DNA-binding domains could be necessary for optimal DNA-binding in these repressors. The overall similarity, however, allows for the construction of a composite model for the DNA-bound conformation of YvoA in which the two DNA-binding domains display a similar orientation than in YydK and FadR (Figure 3B).

Analysis of the composite model and of the protein sequences shows that the wHTH domain in YvoA is even more similar to FadR (35% sequence identity) than to YydK (30% identity; Figure 3C). Two of three residues that are known to specifically recognize the operator sequence in FadR (R35, R45 and H65; FadR numbering) (35,44) are conserved in YvoA (Figure 3C). Moreover, key residues which are suggested to form salt bridge interactions with phosphate groups or to stabilize the positions of the aforementioned arginines in FadR (35) are conserved in YvoA, namely residues E37, S47, T50, R52 and G69 (YvoA numbering, Figure 3C). At the same time, the operator sequence of FadR shows significant similarity to that of YvoA (Table 3) (7,35). In summary, the sequence similarities between FadR and YvoA suggest

Downloaded from https://academic.oup.com/nar/article-abstract/38/7/2485/3100518 by guest on 20 November 2018

that the DNA-binding mode of YvoA resembles that of FadR despite the fact that FadR is a member of a different subfamily of GntRs. Therefore, the FadR/YydK-derived composite model represents a likely conformation of a 1:1 complex between dimeric YvoA and dsDNA.

Table 3. Comparison of DNA operator sequences of YvoA from *B. subtilis* and FadR from *E. coli*

Source	DNA sequence
YvoA operator from *B. subtilis* (7)	TGGTATAGATCA
YvoA/DasR consensus *dre*, palindrome (43)	TGGTCTAGACCA
FadR operator from *E. coli*, palindrome (35)	TGGTCC-GACCA
FadR operator consensus, palindrome (35)	TGGTNN-NACCA

Conserved bases in the YvoA/FadR operator sequences are underlined.

DNA and effector binding require two distinct conformations

The above considerations suggest that YvoA adopts two distinct conformations when bound either to a small molecule effector or to DNA. To investigate the binding properties of these two conformations, we designed two disulfide-bridged mutants that lock YvoA either in the modeled DNA-bound conformation (YvoA-E61C-L242C) or in the conformation that we observe in the crystal structure (resembling the effector-bound induced conformation, YvoA-K24C-G97C) (Figure 4A and B).

The successful production and characterization of the disulfide-bridged mutant YvoA-E61C-L242C (Figure 4A) provides strong evidence that YvoA is able to adopt the inferred DNA-binding conformation. The successful formation of the intermolecular disulfide bridges could be

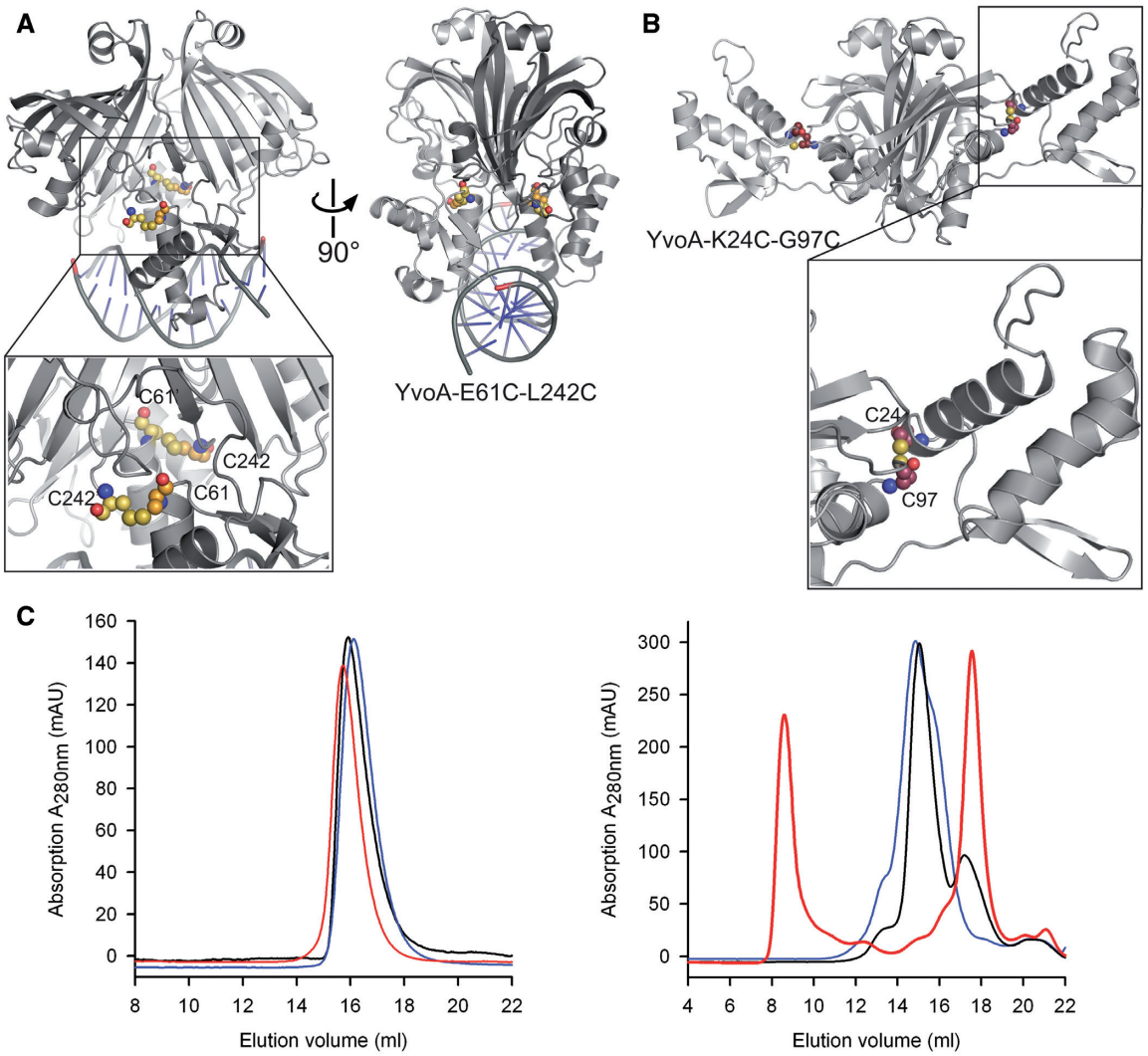

Figure 4. Models of disulfide-bridged YvoA mutants and their DNA-binding properties. (**A**) Model of the homodimeric cystein mutant YvoA-E61C-L242C viewed from two different angles. This model is supposed to represent the DNA-bound conformation leading to repression of YvoA-controlled genes. The inset shows the region around the intermolecular disulfide bridge between C61 and C242′. (**B**) Model of the homodimeric cystein mutant YvoA-K24C-G97C resembling the induced conformation. The inset shows the region around the intramolecular disulfide bridge between C24 and C97. (**C**) Left: gel filtration of free wild-type YvoA (black), YvoA-E61C-L242C (blue), and YvoA-K24C-G97C (red) reveals only small differences in the elution profile. Right: gel filtration of YvoA variants in the presence of dsDNA (18mer) shows major peak shifts. The black line represents wild-type YvoA in the presence of equimolar dsDNA. The blue line shows YvoA-E61C-L242C in excess over dsDNA. The red line represents YvoA-K24C-G97C in the presence of equimolar dsDNA.

Downloaded from https://academic.oup.com/nar/article-abstract/38/7/2485/3100518 by guest on 20 November 2018

confirmed by nonreducing SDS-polyacrylamide gel electrophoresis (PAGE) (data not shown). Isothermal titration of YvoA-E61C-L242C demonstrated its inability to bind GlcNAc-6-P, as anticipated for a non-inducible locked mutant (Table 2, Supplementary Figure S3C). CD spectroscopy and gel filtration experiments showed that the impaired effector binding is not due to a loss of structural integrity (Figure 4C, Supplementary Figure S2). According to our model, this mutant is expected to bind DNA exclusively in a one-to-one complex (one YvoA dimer bound to dsDNA). Indeed, even with a 3.5-fold molar excess of YvoA-E61C-L242C over dsDNA, the protein–DNA complex eluted in a gel filtration experiment as expected for a one-to-one complex in support of the validity of the DNA-bound YvoA model (Figure 4C).

Gel filtration chromatography was also performed with a second YvoA mutant locked in the disulfide-bridged induced conformation (Figure 4B). Again, CD spectroscopy and gel filtration experiments confirmed the structural integrity of this mutant (Figure 4C, Supplementary Figure S2). As anticipated, the mutant YvoA-K24C-G97C was still able to bind GlcNAc-6-P (Table 2, Supplementary Figure S3D). The slightly reduced binding efficiency possibly stems from a reduced accessibility of the effector-binding site in this mutant. Unexpectedly, the mutant YvoA-K24C-G97C was also able to bind DNA (Figure 4C). However, in contrast to wild-type YvoA, the YvoA-K24C-G97C–DNA complex did not elute as a complex of dimeric YvoA plus dsDNA but in the void volume of the column instead, irrespective of whether YvoA was present in excess over DNA (data not shown) or in equimolar concentration (Figure 4C). In this mutant, in which the DNA-binding domains are splayed apart, YvoA appears to bind to two different dsDNA molecules and at the same time the two operator half-sites interact with two different YvoA dimers. As a result, a linear polymer is formed composed of alternating YvoA dimers and dsDNA building blocks. Obviously, in this disulfide-bridged conformation, no complex can be formed in which one YvoA dimer binds to a single operator dsDNA.

Further indications that YvoA adopts distinct conformations upon binding to either small molecule effectors or to DNA are obtained with limited proteolysis experiments. When exposed to small amounts of the unspecific serine protease subtilisin, different proteolytic products are observed depending on whether no ligand, dsDNA or GlcNAc-6-P is present (Figure 5, Supplementary Figure S6). In the absence of both dsDNA and GlcNAc-6-P, three stable fragments can be observed in SDS gels. These start with amino acid residues K5, R96 and L86 (residues C-terminal to the scissile bond; marked 'double dagger', 'dagger' and 'asterisk' in Figure 5). The latter two lie in the interdomain region between the DNA-binding domain and the effector-binding domain (α4-L86-α5-R96-β4). In the presence of dsDNA, the fragments that start at L86 and R96 re-occur with R96 becoming the most abundant. In contrast, when GlcNAc-6-P is present, a fourth band starting with residue R70 emerges. R70 is located in the loop connecting

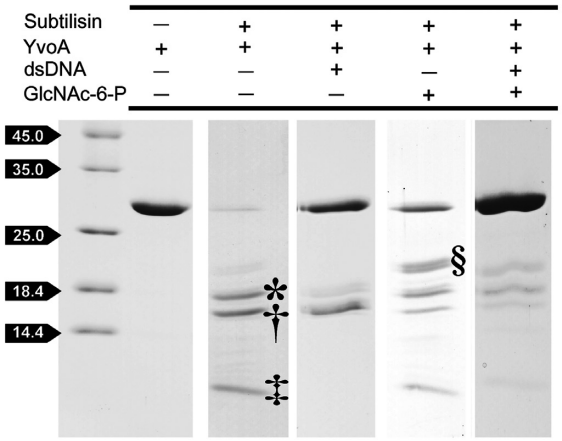

Figure 5. Limited proteolysis assay of YvoA. YvoA (0.35 mg ml^{-1}, i.e. 6-μM dimer) was incubated for 180 min with 0.014 U mg^{-1} subtilisin in the presence or absence of dsDNA and/or GlcNAc-6-P. 'Double dagger', 'dagger', 'asterisk' and 'section' mark cleavage products starting with the N-terminal residues K5, R96, L86 and R70, respectively. Molecular mass estimates suggest that the fragments R96, L86 and R70 result from a single cleavage event. This is not the case for the K5 fragment, which is further truncated toward the C-terminus. For complete time courses see Supplementary Figure S6.

strand β2 to β3 within the DNA-binding domain of YvoA (marked by 'section' in Figure 5, see also Figure 1A).

Two plausible explanations exist for the emergence of the R70 fragment upon GlcNAc-6-P addition. It is possible that R70 is protected in the ligand-free and in the DNA-bound structure so that no cleavage can occur at this position. Likewise, cleavage at R70 could occur rapidly in all samples but subsequent cleavage at residues R96 and L89 could be slowed down in the presence of the inducer so that the R70 fragment emerges as a stable fragment. The second explanation seems likely since the accessibility of residue R70 should vary considerably in the ligand-free and DNA-bound structure without this being reflected in the observed fragmentation pattern. Moreover, we observe that in the DNA-bound model as well as in the YydK template, from which the model was derived, the interdomain segment containing residues R96 and L89 is disordered and might therefore be preferentially cleaved. In contrast, in the sulfate-bound crystal structure, which we propose to mimic the GlcNAc-6-P-bound structure, the region 77–97 is ordered in agreement with a reduced susceptibility to proteolytic cleavage.

DISCUSSION

Allosteric mechanism of induction

Bacterial repressors function as molecular switches and binding of low-molecular-weight effectors modulate their ability to interact with operator DNA. Following the characterization of two distinct conformational states in YvoA that we propose to describe either effector- or operator-bound YvoA, the question arises: what is the nature of the mechanism that triggers the transition between both conformations? Comparison of the DNA-bound YvoA model and the crystal structure

Downloaded from https://academic.oup.com/nar/article-abstract/38/7/2485/3100518 by guest on 20 November 2018

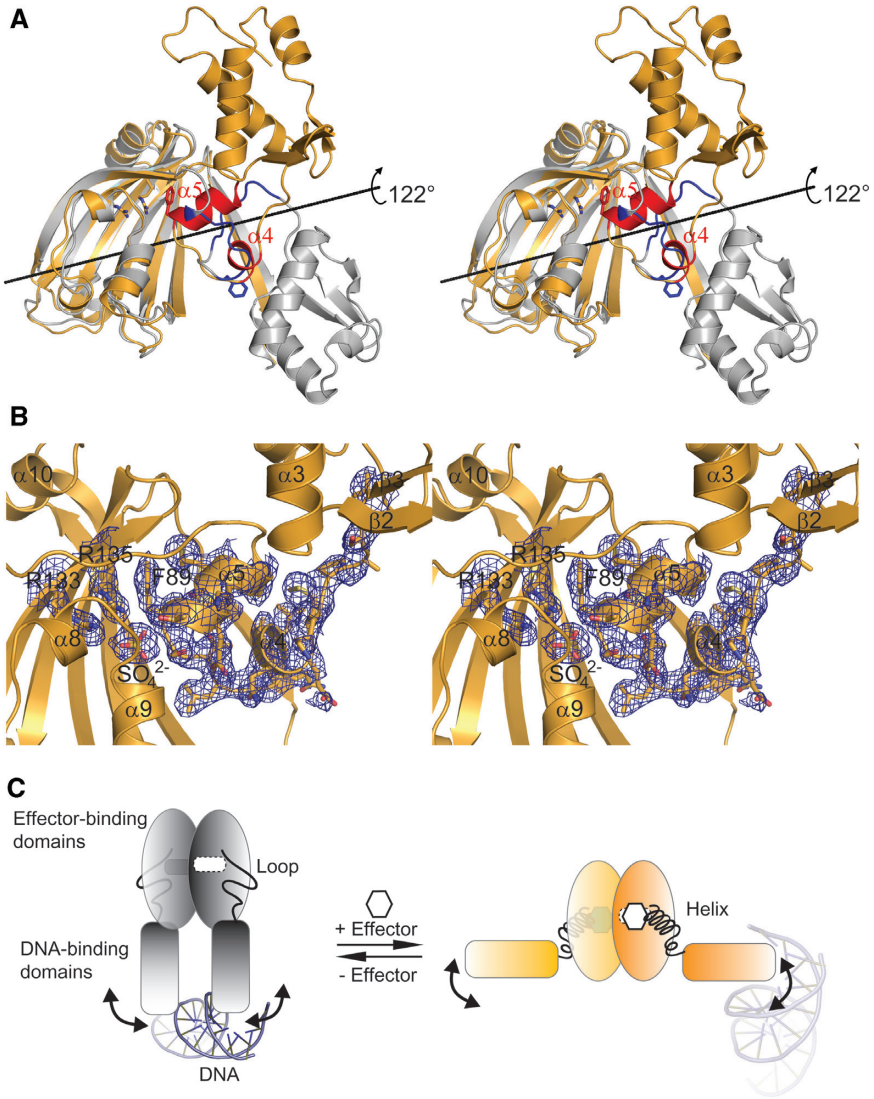

Figure 6. Induction mechanism of YvoA. (**A**) Stereo representation of the allosteric rearrangement in YvoA upon effector binding. The model in the DNA-bound conformation is shown in grey, the crystal structure of induced YvoA in orange. The interdomain loop in the DNA-bound model is highlighted in blue. Upon effector binding, this loop switches conformations and folds into helices α4 and α5 (colored in red). As a consequence, the DNA-binding domain rotates as a rigid body by 122° around the indicated axis. (**B**) Magnified stereo view of helices α4 and α5 in induced YvoA. The σ_A-weighted $2F_o$–F_c electron density map shows well-defined, continuous density for the interdomain linker in YvoA. (**C**) Allosteric mechanism of YvoA induction. In the DNA-binding conformation (in gray), homodimeric YvoA binds DNA with its DNA recognition helices paired together at the dimer interface and binding into successive major grooves. In doing so, YvoA is able to block transcription of any downstream genes. Upon effector (GlcNAc-6-P) binding, the interdomain linker region undergoes a loop-to-helix transition forcing the DNA-binding domains apart in a 'jumping jack'-like motion (orange). YvoA is then not able any more to bind to the same dsDNA duplex with both DNA-binding domains simultaneously, causing de-repression of YvoA-controlled genes.

shows major differences in the region that connects the DNA-binding domain to the effector-binding domain (residues 77–97). In the DNA-bound model, these residues form a partially disordered loop, as apparent from the observed susceptibility of the residues within this loop for proteolysis and the observation that the corresponding YydK residues 82–89 are not visible in the electron density of YydK (PDB code: 3BWG) (Figure 6A). Upon effector binding, these residues undergo a conformational transition that can be described as a loop-to-helix transition. In particular, residues 80–84 and 89–95 switch their conformation and form helices α4 and α5 in the induced-like YvoA crystal structure.

We propose that the negatively charged phosphate group of GlcNAc-6-P (or the sulfate molecule in the crystal structure) triggers this transition. Binding of GlcNAc-6-P to the N-terminus of helix α9 might not just stabilize the dipole moment of this helix but might at the same time induce the formation of helix α5. Upon helix α5 formation, the phosphate becomes sandwiched between the N-termini of both helices with both helix dipoles pointing toward the phosphate (Figures 2B and 6B). Helix α5 formation might concomitantly induce cooperative folding of neighboring helix α4 as a key step in the propagation of the allosteric signal toward the DNA-binding domains. An interesting feature of this

Downloaded from https://academic.oup.com/nar/article-abstract/38/7/2485/3100518 by guest on 20 November 2018

mechanism is that formation of helices α4 and α5 generates internal symmetry within the effector-binding domain (Figure 1B and C) with the 2-fold symmetry axis intersecting with the phosphate/sulfate group bound in the effector-bound conformation. Concurrently with this gain in symmetry, the DNA-binding domains are reoriented and forced apart in a 'jumping jack'-like motion (Figure 6C). The observation that many of the HutC/GntR family members bind phosphate-containing effector molecules suggests that this allosteric induction mechanism may be common to the members of the HutC/GntR family.

Regulatory implications for gene transcription *in vivo*

In analogy to other repressors, such as the tetracycline and lac repressor (15,18), we expected the effector-bound induced conformation to be incompatible with DNA binding. However, this is not the case. This discovery is remarkable when viewed in the context of dual transcription regulators that act as both repressors and activators. This appears to hold true for several regulators implicated in both the transcription of anabolic and catabolic genes such as the *E. coli* FadR regulator and *B. subtilis* arginine repressor/activator AhrC (35,45,46). When FadR binds downstream of the RNA polymerase-binding site within the promoter, it blocks the polymerase and acts as a repressor (35). Conversely, when bound upstream, it promotes binding of the RNA polymerase (35) and acts as an activator. In case of YvoA, one could speculate that yet another mechanism might apply. In addition to blocking transcription through binding to *dre*-operator sites in the above characterized DNA-bound conformation, it is conceivable that YvoA, through binding to two different *dre* sites in the splayed induced conformation, brings two operons together, like for example the *nagAB* and the *nagP* operon located in different regions of the genome, possibly facilitating concomitant transcription of these genes. Thus, YvoA could switch between repressor and activator and thereby rapidly respond to cellular requirements. A clearer picture, however, will have to await additional experimental evidence.

ACCESSION NUMBER

2WV0.

SUPPLEMENTARY DATA

Supplementary Data are available at NAR Online.

ACKNOWLEDGEMENTS

We thank Uwe Müller from BESSY synchrotron (Berlin, Germany) for help with data collection. We are grateful to Caroline Kisker, Hermann Schindelin (RVZ, University of Würzburg) and Norbert Sträter (Center for Biotechnology and Biomedicine, University of Leipzig) for providing access to the spectropolarimeter and ITC equipment. We thank Christian Schmidt for help with the limited proteolysis assays and Madhumati Sevvana for valuable advice during the crystallographic refinement of the structure.

FUNDING

Elitenetzwerk Bayern, BIGSS; and Deutsche Forschungsgemeinschaft, DFG (grant Mu1477/6-1). Funding for open access charge: DFG (grant Mu1477/6-1).

Conflict of interest statement. None declared.

REFERENCES

1. Brückner,R. and Titgemeyer,F. (2002) Carbon catabolite repression in bacteria: choice of the carbon source and autoregulatory limitation of sugar utilization. *FEMS Microbiol. Lett.*, **209**, 141–148.
2. Stülke,J. and Hillen,W. (2000) Regulation of carbon catabolism in *Bacillus* species. *Annu. Rev. Microbiol.*, **54**, 849–880.
3. Rigali,S., Nothaft,H., Noens,E.E., Schlicht,M., Colson,S., Muller,M., Joris,B., Koerten,H.K., Hopwood,D.A., Titgemeyer,F. *et al.* (2006) The sugar phosphotransferase system of Streptomyces coelicolor is regulated by the GntR-family regulator DasR and links N-acetylglucosamine metabolism to the control of development. *Mol. Microbiol.*, **61**, 1237–1251.
4. Reizer,J., Bachem,S., Reizer,A., Arnaud,M., Saier,M.H. Jr. and Stülke,J. (1999) Novel phosphotransferase system genes revealed by genome analysis - the complete complement of PTS proteins encoded within the genome of *Bacillus subtilis*. *Microbiology*, **145**, 3419–3429.
5. Rigali,S., Titgemeyer,F., Barends,S., Mulder,S., Thomae,A.W., Hopwood,D.A. and van Wezel,G.P. (2008) Feast or famine: the global regulator DasR links nutrient stress to antibiotic production by Streptomyces. *EMBO Rep.*, **9**, 670–675.
6. Rigali,S., Schlicht,M., Hoskisson,P., Nothaft,H., Merzbacher,M., Joris,B. and Titgemeyer,F. (2004) Extending the classification of bacterial transcription factors beyond the helix-turn-helix motif as an alternative approach to discover new cis/trans relationships. *Nucleic Acids Res.*, **32**, 3418–3426.
7. You,C., Lu,H., Sekowska,A., Fang,G., Wang,Y., Gilles,A.M. and Danchin,A. (2005) The two authentic methionine aminopeptidase genes are differentially expressed in *Bacillus subtilis*. *BMC Microbiol.*, **5**, 57.
8. Vincent,F., Davies,G.J. and Brannigan,J.A. (2005) Structure and kinetics of a monomeric glucosamine 6-phosphate deaminase: missing link of the NagB superfamily? *J. Biol. Chem.*, **280**, 19649–19655.
9. Vincent,F., Yates,D., Garman,E., Davies,G.J. and Brannigan,J.A. (2004) The three-dimensional structure of the N-acetylglucosamine-6-phosphate deacetylase, NagA, from *Bacillus subtilis*: a member of the urease superfamily. *J. Biol. Chem.*, **279**, 2809–2816.
10. Bates,C.J. and Pasternak,C.A. (1965) Further studies on the regulation of amino sugar metabolism in *Bacillus subtilis*. *Biochem. J.*, **96**, 147–154.
11. Haydon,D.J. and Guest,J.R. (1991) A new family of bacterial regulatory proteins. *FEMS Microbiol. Lett.*, **63**, 291–295.
12. van Aalten,D.M., DiRusso,C.C., Knudsen,J. and Wierenga,R.K. (2000) Crystal structure of FadR, a fatty acid-responsive transcription factor with a novel acyl coenzyme A-binding fold. *EMBO J.*, **19**, 5167–5177.
13. Aravind,L. and Anantharaman,V. (2003) HutC/FarR-like bacterial transcription factors of the GntR family contain a small molecule-binding domain of the chorismate lyase fold. *FEMS Microbiol. Lett.*, **222**, 17–23.
14. Gallagher,D.T., Mayhew,M., Holden,M.J., Howard,A., Kim,K.J. and Vilker,V.L. (2001) The crystal structure of chorismate lyase shows a new fold and a tightly retained product. *Proteins*, **44**, 304–311.

Downloaded from https://academic.oup.com/nar/article-abstract/38/7/2485/3100518 by guest on 20 November 2018

15. Saenger,W., Orth,P., Kisker,C., Hillen,W. and Hinrichs,W. (2000) The Tetracycline repressor – a paradigm for a biological switch. *Angew. Chem. Int. Ed. Engl.*, **39**, 2042–2052.
16. Gorelik,M., Lunin,V.V., Skarina,T. and Savchenko,A. (2006) Structural characterization of GntR/HutC family signaling domain. *Protein Sci.*, **15**, 1506–1511.
17. Rezacova,P., Krejcirikova,V., Borek,D., Moy,S.F., Joachimiak,A. and Otwinowski,Z. (2007) The crystal structure of the effector-binding domain of the trehalose repressor TreR from *Bacillus subtilis* 168 reveals a unique quarternary assembly. *Proteins*, **69**, 679–682.
18. Bell,C.E. and Lewis,M. (2000) A closer view of the conformation of the Lac repressor bound to operator. *Nat. Struct. Biol.*, **7**, 209–214.
19. Lewis,M., Chang,G., Horton,N.C., Kercher,M.A., Pace,H.C., Schumacher,M.A., Brennan,R.G. and Lu,P. (1996) Crystal structure of the lactose operon repressor and its complexes with DNA and inducer. *Science*, **271**, 1247–1254.
20. Kisker,C., Hinrichs,W., Tovar,K., Hillen,W. and Saenger,W. (1995) The complex formed between Tet repressor and tetracycline-Mg2+ reveals mechanism of antibiotic resistance. *J. Mol. Biol.*, **247**, 260–280.
21. Resch,M., Roth,H.M., Kottmair,M., Sevvana,M., Bertram,R., Titgemeyer,F. and Muller,Y.A. (2009) Cloning, expression, purification, crystallization and preliminary X-ray diffraction analysis of YvoA from *Bacillus subtilis*. *Acta Crystallogr. Sect. F*, **65**, 410–414.
22. Wang,W. and Malcolm,B.A. (1999) Two-stage PCR protocol allowing introduction of multiple mutations, deletions and insertions using QuikChange site-directed mutagenesis. *Biotechniques*, **26**, 680–682.
23. Van Duyne,G.D., Standaert,R.F., Karplus,P.A., Schreiber,S.L. and Clardy,J. (1993) Atomic structures of the human immunophilin FKBP-12 complexes with FK506 and rapamycin. *J. Mol. Biol.*, **229**, 105–124.
24. Wiseman,T., Williston,S., Brandts,J.F. and Lin,L.N. (1989) Rapid measurement of binding constants and heats of binding using a new titration calorimeter. *Anal. Biochem.*, **179**, 131–137.
25. Kabsch,W. (1993) Automatic processing of rotation diffraction data from crystals of initially unknown symmetry and cell constants. *J. Appl. Crystallogr.*, **26**, 795–800.
26. Vonrhein,C., Blanc,E., Roversi,P. and Bricogne,G. (2007) Automated structure solution with autoSHARP. *Methods Mol. Biol.*, **364**, 215–230.
27. Emsley,P. and Cowtan,K. (2004) Coot: model-building tools for molecular graphics. *Acta Crystallogr. D Biol. Crystallogr.*, **60**, 2126–2132.
28. Murshudov,G.N., Vagin,A.A. and Dodson,E.J. (1997) Refinement of macromolecular structures by the maximum-likelihood method. *Acta Crystallogr. D Biol. Crystallogr.*, **53**, 240–255.
29. Winn,M.D., Isupov,M.N. and Murshudov,G.N. (2001) Use of TLS parameters to model anisotropic displacements in macromolecular refinement. *Acta Crystallogr. D Biol. Crystallogr.*, **57**, 122–133.
30. Painter,J. and Merritt,E.A. (2005) A molecular viewer for the analysis of TLS rigid-body motion in macromolecules. *Acta Crystallogr. D Biol. Crystallogr.*, **61**, 465–471.
31. Painter,J. and Merritt,E.A. (2006) Optimal description of a protein structure in terms of multiple groups undergoing TLS motion. *Acta Crystallogr. D Biol. Crystallogr.*, **62**, 439–450.
32. Howlin,B., Butler,S.A., Moss,D.S., Harris,G.W. and Driessen,H.P.C. (1993) TLSANL: TLS parameter-analysis program for segmented anisotropic refinement of macromolecular structures. *J. Appl. Crystallogr.*, **26**, 622–624.
33. DeLano,W. (2003) *The PyMOL Molecular Graphics System*. DeLano Scientific LLC, San Carlos, CA.
34. Lambert,C., Leonard,N., De Bolle,X. and Depiereux,E. (2002) ESyPred3D: prediction of proteins 3D structures. *Bioinformatics*, **18**, 1250–1256.
35. Xu,Y., Heath,R.J., Li,Z., Rock,C.O. and White,S.W. (2001) The FadR.DNA complex. Transcriptional control of fatty acid metabolism in *Escherichia coli*. *J. Biol. Chem.*, **276**, 17373–17379.
36. CCP4 (1994) The CCP4 suite: programs for protein crystallography. *Acta Crystallogr. D Biol. Crystallogr.*, **50**, 760–763.
37. Holm,L., Kaariainen,S., Rosenstrom,P. and Schenkel,A. (2008) Searching protein structure databases with DaliLite v.3. *Bioinformatics*, **24**, 2780–2781.
38. Rigali,S., Derouaux,A., Giannotta,F. and Dusart,J. (2002) Subdivision of the helix-turn-helix GntR family of bacterial regulators in the FadR, HutC, MocR, and YtrA subfamilies. *J. Biol. Chem*, **277**, 12507–12515.
39. Nishitani,Y., Maruyama,D., Nonaka,T., Kita,A., Fukami,T.A., Mio,T., Yamada-Okabe,H., Yamada-Okabe,T. and Miki,K. (2006) Crystal structures of N-acetylglucosamine-phosphate mutase, a member of the alpha-D-phosphohexomutase superfamily, and its substrate and product complexes. *J. Biol. Chem.*, **281**, 19740–19747.
40. Copley,R.R. and Barton,G.J. (1994) A structural analysis of phosphate and sulphate binding sites in proteins. Estimation of propensities for binding and conservation of phosphate binding sites. *J. Mol. Biol.*, **242**, 321–329.
41. Hol,W.G. (1985) The role of the alpha-helix dipole in protein function and structure. *Prog. Biophys. Mol. Biol.*, **45**, 149–195.
42. Hol,W.G., van Duijnen,P.T. and Berendsen,H.J. (1978) The alpha-helix dipole and the properties of proteins. *Nature*, **273**, 443–446.
43. Colson,S., Stephan,J., Hertrich,T., Saito,A., van Wezel,G.P., Titgemeyer,F. and Rigali,S. (2007) Conserved *cis*-acting elements upstream of genes composing the chitinolytic system of streptomycetes are DasR-responsive elements. *J. Mol. Microbiol. Biotechnol.*, **12**, 60–66.
44. van Aalten,D.M., DiRusso,C.C. and Knudsen,J. (2001) The structural basis of acyl coenzyme A-dependent regulation of the transcription factor FadR. *EMBO J.*, **20**, 2041–2050.
45. Garnett,J.A., Marincs,F., Baumberg,S., Stockley,P.G. and Phillips,S.E. (2008) Structure and function of the arginine repressor-operator complex from *Bacillus subtilis*. *J. Mol. Biol.*, **379**, 284–298.
46. Miller,C.M., Baumberg,S. and Stockley,P.G. (1997) Operator interactions by the *Bacillus subtilis* arginine repressor/activator, AhrC: novel positioning and DNA-mediated assembly of a transcriptional activator at catabolic sites. *Mol. Microbiol.*, **26**, 37–48.
47. Diederichs,K. and Karplus,P.A. (1997) Improved R-factors for diffraction data analysis in macromolecular crystallography. *Nat. Struct. Biol.*, **4**, 269–275.
48. Laskowski,R.A., MacArthur,M.W., Moss,D.S. and Thornton,J.M. (1993) PROCHECK: a program to check the stereochemical quality of protein structures. *J. Appl. Crystallogr.*, **26**, 283–291.

Downloaded from https://academic.oup.com/nar/article-abstract/38/7/2485/3100518 by guest on 20 November 2018